



This is a repository copy of *Optimal fast charging of lithium ion batteries: between model-based and data-driven methods*.

White Rose Research Online URL for this paper:

<https://eprints.whiterose.ac.uk/209066/>

Version: Accepted Version

---

**Article:**

Tucker, G., Drummond, R. and Duncan, S.R. (2023) Optimal fast charging of lithium ion batteries: between model-based and data-driven methods. *Journal of The Electrochemical Society*, 170 (12). 120508. ISSN 0013-4651

<https://doi.org/10.1149/1945-7111/ad0ccd>

---

© 2023 The Authors. Except as otherwise noted, this author-accepted version of a journal article published in *Journal of The Electrochemical Society* is made available via the University of Sheffield Research Publications and Copyright Policy under the terms of the Creative Commons Attribution 4.0 International License (CC-BY 4.0), which permits unrestricted use, distribution and reproduction in any medium, provided the original work is properly cited. To view a copy of this licence, visit <http://creativecommons.org/licenses/by/4.0/>

**Reuse**

This article is distributed under the terms of the Creative Commons Attribution (CC BY) licence. This licence allows you to distribute, remix, tweak, and build upon the work, even commercially, as long as you credit the authors for the original work. More information and the full terms of the licence here:

<https://creativecommons.org/licenses/>

**Takedown**

If you consider content in White Rose Research Online to be in breach of UK law, please notify us by emailing [eprints@whiterose.ac.uk](mailto:eprints@whiterose.ac.uk) including the URL of the record and the reason for the withdrawal request.



[eprints@whiterose.ac.uk](mailto:eprints@whiterose.ac.uk)  
<https://eprints.whiterose.ac.uk/>

# Optimal fast charging of lithium ion batteries: Between model-based and data-driven methods

George Tucker<sup>a</sup>, Ross Drummond<sup>b,\*</sup>, Stephen R. Duncan<sup>a</sup>

<sup>a</sup>*Department of Engineering Science, University of Oxford, Parks Road, Oxford, OX1 3PJ, UK*

<sup>b</sup>*Department of Automatic Control and Systems Engineering, University of Sheffield, Mappin St, Sheffield, S1 3JD, UK*

---

## Abstract

Delivering lithium ion batteries capable of fast charging without suffering from accelerated degradation is an important milestone for transport electrification. Recently, there has been growing interest in applying data-driven methods for optimising fast charging protocols to avoid accelerated battery degradation. However, such data-driven approaches suffer from a lack of robustness, explainability and generalisability, which has hindered their wide-spread use in practice. To address this issue, this paper proposes a method to interpret the fast charging protocols of data-driven algorithms as the solutions of a model-based optimal control problem. This hybrid approach combines the power of data-driven methods for predicting battery degradation with the flexibility and optimality guarantees of the model-based approach. The results highlight the potential of the proposed hybrid approach for generating fast charging protocols. In particular, for fast charging to 80% state-of-charge in 10 minutes, the proposed approach was predicted to increase the cycle life from 912 to 1078 cycles when compared against a purely data-driven approach.

*Keywords:* Lithium-ion batteries, degradation modelling, fast charging.

---

## 1. Introduction

The transition towards full electric transportation and grid storage is increasing the pressure to deliver improved lithium-ion batteries, as their combination of high energy and power densities, long lifespans and low costs have made them the standard energy storage device for electric transportation. However, current battery performance is insufficient for most intensive applications requiring fast charging. As defined by the US Department of Energy, extreme fast charging requires a fresh cell to achieve a fast charged specific energy of 180 Wh/kg and for the loss in capacity to be less than 20% after 500 cycles [1, 2], specifications beyond the capabilities of today's commercially available lithium ion cells. Achieving these performance targets in a scalable and economic manner will require advances in both battery materials and management, as reviewed in [3, 4, 5].

Most battery management algorithms are based on a battery model that can be used to make predictions about the response of a cell. A variety of battery models now exist, ranging in scale from simple equivalent circuits [6] to electrochemical models such as the Doyle-Fuller-Newman model [7]. Battery models have proven highly successful in a number of applications, including state-of-charge estimation [8], electrode design (by linking the model parameters to cell performance [9, 10] and setting up thick [11] and graded [12] electrodes) and optimising fast charging protocols. Various solutions to the fast charging optimisation problem have been proposed, including those based upon nonlinear programming and optimal control theory. Examples include the early works of [13, 14] and more modern approaches, such as [15] which used the measure-moment approach to search over discontinuous charging strategies, [16] which included thermal and ageing dynamics, [17] which applied Bayesian optimisation to accelerate the computation, and [18] which implemented reinforcement learning. These methods are able to generate optimal fast charging protocols (often called reference trajectories) but when the cell deviates from these policies (due to unmodelled dynamics

---

\*Corresponding author.

*Email addresses:* [gfttucker@gmail.com](mailto:gfttucker@gmail.com) (George Tucker), [ross.drummond@sheffield.ac.uk](mailto:ross.drummond@sheffield.ac.uk) (Ross Drummond), [stephen.duncan@eng.ox.ac.uk](mailto:stephen.duncan@eng.ox.ac.uk) (Stephen R. Duncan)

for instance) then feedback control is needed to apply corrections and push the battery back towards the reference. Feedback control schemes for fast charging include the reference governors of [19], model predictive control [20, 21] and its extension with deep learning [22], the model inversion strategy with output tracking from [23], the adaptive schemes of [24] that are able to accommodate faults and the switching schemes for constraint satisfaction [25] and following different operating modes [26]. Satisfying the problem constraints are key in these optimal strategies [27], with the most significant constraint being the one for lithium plating, but there are others, including for mechanical stress [28]. This has motivated several modelling studies on quantifying, or at least visualising, the onset of lithium plating, with characterisation studies including [29, 30] and the voltage based scheme of [31]. Critical to the success of these schemes is the appropriateness of the model (if the model is too complex, then it adds complexity to the optimal control problem, if it is too simple then the predictions do not capture the key effects). The impact of this trade-off was explored in the sensitivity analysis of [32] which examined how changes in the model parameters, such as the number of active particles, affects its suitability for generating optimal trajectories. More recently, there has been a push towards going beyond the numerical analysis of these fast charging problems and, instead, develop an understanding of the solution structures by examining the optimality conditions. This has led to the development of analytical solutions for many fast charging problems. In particular, using the single particle model, it was shown in [33, 34] that the switching strategies that have proven popular, as used in [26] for instance, are in fact optimal under certain problem assumptions. This idea was generalised in [35] where it was shown that such switching policies, referred to as “bang-and-ride” control, are optimal for the broad class of monotone optimal control problem, which includes many fast charging problems as special cases. Such studies provide the theoretical framework to characterise the solutions of optimal fast charging protocols analytically and to explain why the popular switching strategies perform so well in experiments, even though they are relatively simple.

One area where current battery models have struggled is in predicting battery degradation. While several battery degradation models have been proposed, their predictions have received only limited validation on rich, real-world data and methods to train them efficiently have not yet been established. In response to the challenges faced in implementing and training battery degradation models, there has been growing interest in *data-driven* algorithms, including [17, 36]. Compared to model-based methods, data-driven approaches are trained by extracting features directly from the data, and as battery data has become increasingly available, the performance of these algorithms has steadily improved. Since they are not based on any underlying physical model, data-driven methods can avoid the inherent biases of models and have demonstrated impressive results, especially for predicting knee points in battery cycling data, such as in [37] where accuracy levels of 88–90% were reported even when only the first 3-5 cycles were used for the predictions.

However, data-driven algorithms suffer from limitations that have slowed down their deployment to the battery management and control systems used in practice. For example, these algorithms suffer from an inability to generalise to situations outside of their training data (which is typically cycling data from controlled lab settings that are not necessarily representative of real-world usage [38]). To perform at their best, these algorithms require ‘big data’, but data on this scale is not currently available for batteries [39] because of the extended times and costs needed to run experiments. The large datasets that do exist are predominantly owned by electric vehicle (EV) manufacturers, so they are not open-source and not available to researchers. Data-driven algorithms also suffer from a lack of robustness, which makes it difficult for them to adapt to changing setups (such as when a new cell type is adopted or when the sampling time of the algorithm is updated) without full retraining. By contrast, adapting a model-based method typically involves recomputing the solution with some newly identified model parameters. By operating as a black-box, data-driven methods also suffer from a lack of explainability (meaning an inability of the algorithm to justify its proposed actions), an important consideration for EVs as they are safety critical systems; an EV shutting off power on a busy road because of a decision made by a data-driven algorithm could place users at risk.

For these reasons, it is becoming increasingly apparent that data-driven algorithms need to inherit some of the benefits of model-based methods if they are to be safely deployed to practical settings. Namely, they should be explainable (to improve reliability and reduce the likelihood of unexpected events), generalisable (meaning an ability to adapt to changes in the system setup) and robust (so that they can be guaranteed to work in practice), while still retaining the benefits of the data-driven framework, chiefly an ability to learn battery degradation.

This fusion between model-based and data-driven methods is the problem considered in this paper, with a model-based interpretation of the fast-charging protocols of [36] given. In particular, the main contributions of this paper are:

1. A method to generate fast charging protocols using model-based control optimised on the data-driven protocols of [36].
2. A validation of the proposed method and models using the data of [36].
3. An error-free discretisation in time for the cell thermal dynamics is introduced.

The paper proposes model-based interpretations of the newly emerging data-driven methods for battery management and control. The goal is to combine the ability of the data-driven approach for learning battery degradation with the explainability, robustness and generalisability of the model-based approach. We do this by focusing on interpreting the fast charging protocols of [36], that were derived by a data-driven method, in terms of an optimal control problem involving an electrical and thermal model of the cell. The data and results of [36] were chosen for reference as, at the time of writing, it was considered to be the richest available fast charging data-set capable of linking the cell's cycle life to its fast charging protocol.

The specific problem considered in this work builds upon that of [36] where a multi-stage fast charging protocol [40] was sought to minimise cell degradation. The considered charging protocol optimised here is defined to charge the cell from 0% to 80% SOC in 10 minutes in four constant-current steps, with the duration of each charging step being the time taken to increase the state-of-charge by 20%.

The main similarities and differences between Attia et al. [36] and the presented work are:

- In [36], a machine learning model was developed to estimate the cycles-to-failure of a cell from the data of its first 100 charging cycles using the same charging protocol. Our work developed a predictor for the cycles-to-failure from the dynamical states and charging rates of the first cycle rather than the first 100 cycles, as defined in Equation (26).
- Attia et al. [36] generated a rich data-set containing a large number of cells under different fast charging protocols and cycled them with this same protocol 100 times. In this work, this data-set was used to train an electro-thermal model of the batteries during fast charging (Equation (10)) as well as the cycles-to-failure predictor of Equation (26) based upon the state and current values of this model. No such model was estimated in [36], and the results of Table 4 highlight the benefits of using models for solving fast charging optimisation problems.
- Using the identified model of Equation (10), the optimisation problem of Equation (16) was solved to find the multi-stage constant-current charging protocol to maximise the predicted cycles-to-failure. With this approach, the optimiser could efficiently search over all charging currents satisfying the problem constraints. This contrasted with the purely data-driven method of Attia et al. [36] which could only search over up to nine distinct charging rates during each charging step.

The proposed method is designed to be “*hybrid*” in the sense that it uses the data to learn degradation metrics and the model to improve the optimisation. By mixing data-driven and model-based methods in this way, the proposed approach is predicted to bring superior results compared to the purely data-driven approach of [36]. Specifically, the learned model predicts an increase in the maximum cycle-life-failure from 912 to 1078 compared against the data-driven method of [36]. This increase in cycle life is obtained by exploiting the model's ability to optimise over trajectories, a feature lacking from data-driven methods such as that used in [36]. As well, as increasing the cycle-life, the proposed approach has additional benefits, such as an ability to generalise (for example to account for a change in the sampling time) and learn representations of the ‘black-box’ degradation models, such as that found in [36], in terms of the model's states during the fast charge.

The underlying theme of this work is that linking data-driven and model-based control methods can lead to significant gains for battery control and management problems, such as generating fast charging protocols. By compensating for the weaknesses of each method, a hybrid approach has the potential to lead to new gains in both performance and robustness.

## 2. Cell modelling

To apply optimal control to the ‘A123 Systems APR18650M1A’ cell data of [36], a thermal and voltage model was first developed.

## 2.1. Electrical Model

A simple equivalent circuit model of the form of Figure 1 was used to describe the cell's electrical response.

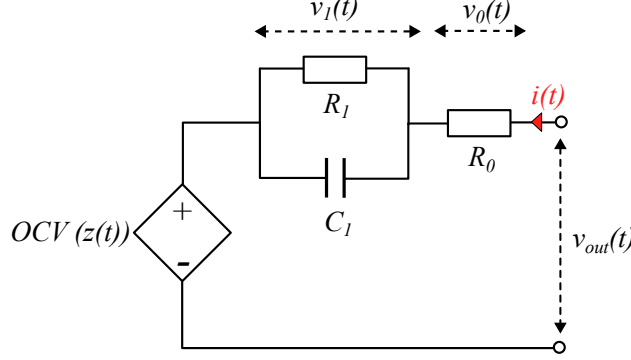


Figure 1: Equivalent circuit model of a cell with one RC pair.

The associated dynamics of this circuit model are

$$\dot{v}_1(t) = -\frac{1}{R_1 C_1} v_1(t) + \frac{1}{C_1} i(t), \quad (1a)$$

$$\dot{z}(t) = \frac{i(t)}{Q}, \quad (1b)$$

with  $z(t)$  being the cell's state-of-charge,  $i(t)$  the applied current (A),  $Q$  the cell capacitance (As),  $v_1$  the voltage drop (V) across the RC-pair of Figure 1 with  $R_1$ ,  $C_1$  being, respectively, the resistance and capacitance.

The voltage of the model was

$$v_{out}(t) = OCV(z(t)) + v_1(t) + R_0 i(t) \quad (2)$$

with  $OCV(z(t))$  being the open circuit voltage,  $v_1(t)$  the voltage drop over the RC pair and  $R_0 i(t)$  the ohmic term. Throughout the paper, the notation that a charging current is positive (so that the cell charges when  $i(t) > 0$ ) is adopted.

It is assumed that the electrical parameters ( $R_1, C_1, R_0$ ) of the circuit in Figure 1 remain constant throughout charging. It is noted that in reality, the model parameters would vary with state-of-charge, temperature, and the cell's age [41]. The effects of varying  $R_0$  were considered and are discussed in Appendix A. Compared to other battery models, in particular electrochemical ones such as the Doyle-Fuller-Newman (DFN) [7, 42], it is acknowledged that the circuit model of Figure 1 is simple. However, since the main focus of this paper is on linking model-based and data-driven control for fast-charging, this simple model was sufficient to allow an accurate parameterisation from the data, while also being sufficiently computationally efficient.

## 2.2. Thermal model

Considering heat generation rates, the temperature of the cell was modelled as

$$m c_p \dot{T}(t) = P_{generated}(t) - P_{emitted}(t), \quad (3)$$

with  $m$  being the cell mass (kg),  $c_p$  the specific heat capacity ( $\text{Jkg}^{-1}\text{K}^{-1}$ ) and  $T$  the cell temperature (K) (assumed to be uniform throughout the cell). Here, ohmic heating was taken to be the sole source of the power heating the cell,  $P_{generated}(t)$  [43], so

$$P_{generated}(t) = i(t)(v_{out}(t) - OCV(z(t))), \quad (4)$$

$$= i(t)(R_0 i(t) + v_1(t)), \quad (5)$$

and convective heat transfer was assumed for the power dissipated by the cell to the surroundings,  $P_{emitted}(t)$ , so

$$P_{emitted}(t) = hA(T(t) - T_{amb}), \quad (6)$$

with  $h$  being the convective heat transfer coefficient ( $\text{Wm}^{-2}\text{K}^{-1}$ ),  $A$  the cell's surface area ( $\text{m}^2$ ) and  $T_{amb}$  the ambient room temperature (K), which was assumed to be constant.

In practice, lithium ion batteries experience several additional modes of heat generation, such as from entropy change effects and side-reactions [43, 41]. However, for fast charging, it has been shown that the Ohmic heat generation of Equation (4) is the dominant source of heat generation [44]. Therefore, these other heat generation terms were neglected in the simple model of Equation (5). Likewise, in our preliminary testing, it was found that radiative heat transfer was small in comparison to convective heat transfer, and so only convective heat emission was considered in Equation (6).

By defining the temperature difference between the cell and the ambient air as  $\Delta T(t) = T(t) - T_{amb}$ , the following thermal dynamics are obtained

$$\Delta \dot{T}(t) = -\frac{hA}{mc_p} \Delta T(t) + \frac{R_0}{mc_p} i(t)^2 + \frac{1}{mc_p} v_1(t)i(t). \quad (7)$$

### 2.3. Model discretisation

Combining Equations (1a), (1b), and (7) gives a state space representation of the combined electrical and thermal models

$$\begin{bmatrix} \dot{v}_1(t) \\ \dot{z}(t) \\ \Delta \dot{T}(t) \end{bmatrix} = \begin{bmatrix} -\frac{1}{R_1 C_1} & 0 & 0 \\ 0 & 0 & 0 \\ 0 & 0 & -\frac{hA}{mc_p} \end{bmatrix} \begin{bmatrix} v_1(t) \\ z(t) \\ \Delta T(t) \end{bmatrix} + \begin{bmatrix} \frac{1}{C_1} & 0 & 0 \\ \frac{1}{Q} & 0 & 0 \\ 0 & \frac{R_0}{mc_p} & \frac{1}{mc_p} \end{bmatrix} \begin{bmatrix} i(t) \\ i(t)^2 \\ v_1(t)i(t) \end{bmatrix}, \quad (8)$$

with outputs  $v_{out}(t) = OCV(z(t)) + v_1(t) + R_0 i(t)$ , and  $T(t) = T_{amb} + \Delta T(t)$ . For ease of notation, this system is expressed as

$$\begin{bmatrix} \dot{v}_1(t) \\ \dot{z}(t) \\ \Delta \dot{T}(t) \end{bmatrix} = \begin{bmatrix} -\lambda_1 & 0 & 0 \\ 0 & 0 & 0 \\ 0 & 0 & -\lambda_2 \end{bmatrix} \begin{bmatrix} v_1(t) \\ z(t) \\ \Delta T(t) \end{bmatrix} + \begin{bmatrix} b_1 & 0 & 0 \\ b_2 & 0 & 0 \\ 0 & b_3 & b_4 \end{bmatrix} \begin{bmatrix} i(t) \\ i(t)^2 \\ v_1(t)i(t) \end{bmatrix}. \quad (9)$$

The model equations outlined above are defined in continuous time, however, in order for the model to compare the data of [36], which is sampled at discrete time steps, the dynamics had to be converted into a discrete time form. By integrating the thermal and electrical dynamics of (7) and (1), the following discrete-time system was obtained

$$\begin{bmatrix} v_1[k+1] \\ z[k+1] \\ \Delta T[k+1] \end{bmatrix} = \begin{bmatrix} e^{-\lambda_1 \Delta t[k]} & 0 & 0 \\ 0 & 1 & 0 \\ 0 & 0 & e^{-\lambda_2 \Delta t[k]} \end{bmatrix} \begin{bmatrix} v_1[k] \\ z[k] \\ \Delta T[k] \end{bmatrix} + \begin{bmatrix} \beta_1 & 0 & 0 \\ \beta_2 & 0 & 0 \\ 0 & \beta_3 & \beta_4 \end{bmatrix} \begin{bmatrix} i[k] \\ i[k]^2 \\ v_1[k]i[k] \end{bmatrix} \quad (10)$$

where

$$\beta_1 = \frac{b_1}{\lambda_1} (1 - e^{-\lambda_1 \Delta t[k]}), \quad (11a)$$

$$\beta_2 = b_2 \Delta t[k], \quad (11b)$$

$$\beta_3 = \left( \frac{b_3}{\lambda_2} + \frac{b_1 b_4}{\lambda_1 \lambda_2} \right) (1 - e^{-\lambda_2 \Delta t[k]}) - \frac{b_1 b_4}{\lambda_1 (\lambda_2 - \lambda_1)} (e^{-\lambda_1 \Delta t[k]} - e^{-\lambda_2 \Delta t[k]}), \quad (11c)$$

$$\beta_4 = \frac{b_4}{\lambda_2 - \lambda_1} (e^{-\lambda_1 \Delta t[k]} - e^{-\lambda_2 \Delta t[k]}), \quad (11d)$$

and  $\Delta t[k]$  is the time-step at time index  $k$  and square brackets are used to indicate the time step. Throughout, the

applied current is assumed to be zero-order hold

$$i(t) = i[k] \forall t \in \left[ \sum_{j=0}^{k-1} \Delta t[j], \sum_{j=0}^k \Delta t[j] \right),$$

so that the current is constant throughout the sampling interval. To relate the model to the data of [36], a time-varying time step was adopted. In particular, in [36] the time-step was defined so that the cell was charged by a set portion of the cell capacity, namely  $pQ$ , during each sampling interval  $\Delta t[k]$ , where  $p$  is defined as the proportion of the cells total capacity to be charged per step. Since the stored capacity is a function of the applied current, the time-steps followed

$$\Delta t[k] = \frac{pQ}{i[k]}, \quad (12)$$

which vary with the applied current  $i[k]$  with  $K$  being the total number of time steps. In keeping with the protocols of [36],  $K = 4$  and  $p = 0.2$  in this paper.

Since the electrical model dynamics of (1) are linear, their discretisation can be readily obtained by simple integration. This is not true for the thermal model of (7), due to the bi-linear heat generation term  $v_1(t)i(t)$  - even if a zero order hold is assumed on the current  $i(t)$ , this does not imply the relaxation voltage  $v_1(t)$  will also be constant during the sample interval, and so neither will  $v_1(t)i(t)$ . Normally, as in [45, Appendix 1] and [46] which discretised the model in [47], thermal dynamics such as (7) are discretised using an Euler approximation

$$\frac{d\Delta T(t)}{dt} \approx \frac{\Delta T[k+1] - \Delta T[k]}{\Delta t[k]}. \quad (13)$$

However, this is not what is done here, as the resulting approximation errors from using (13) were found to be large for the long time-steps ( $\approx 200$ s) of [36]. Instead, an exact solution for the discretisation of the thermal model of (7) was obtained, Equation (10), that took into account the fact that the relaxation voltage  $v_1(t)$  changes during a sampling instant. This exact discretisation is the first main result of this paper and its full derivation is given in Appendix B.

The expression for the voltage at each sampling time is

$$v_{out}[k] = OCV(z[k]) + v_1[k] + R_0 i[k]. \quad (14)$$

For the optimisation problems of (16), it was also found that the voltage immediately before the sampling point, defined here as

$$v_{out}[k - \delta t] = OCV(z[k]) + v_1[k] + R_0 i[k - 1], \quad (15)$$

had to be constrained to prevent infeasible solutions. Here, the notation  $[k - \delta t]$  indicates the time immediately before sampling point  $k$ .

## 2.4. Parameter estimation

The model parameters (in Table 1) were estimated using the data from [36]. The data of [36] is divided into five ‘batches’ of up to 48 cells each, or fewer if the experiment failed or the cycle life prediction was anomalous. Data is available for the input current and output voltage of the cells within the first four batches, which were repeatedly charged and discharged (cycled) at least 100 times. Temperature data is also available in [36] for the fifth batch. Cells within batch 5 were cycled to failure and the number of cycles before failure was tabulated for each cell and charging protocol [36]. To parameterise the model (10), only the first cycle of each charging protocol was considered so that all of the data used to train the model was from ‘new’ cells with the same, minimal, degradation.

### 2.4.1. Estimating the electrical model parameters

For parameterising the electrical model, batch 1 from [36] was reserved for training the model; this consisted of 46 cells each with a unique charging current protocol. Batch 5 was used for testing the model and any cells with charging protocols matching those in the training set were removed from the testing set prior to model testing. Additionally,

some of the samples had data missing for extended periods of times and were removed from the dataset. The final testing set thus consisted of 7 cells, each with a unique charging protocol. Batches 2-4 contained cells charged with protocols that were identical or very similar to batch 1 so were not used in training or testing.

$R_0$  was found by observing step changes in voltage at the same time as step changes in current.  $R_0$  was then taken to be the magnitude of the step change in voltage divided by the magnitude of the step change in current [48]. It was assumed that  $R_0$  did not vary with SOC (see Appendix A) and the model value for  $R_0$  was found by taking an average of the  $R_0$  values from step changes across the training set. This value is given in Table 1.

$R_1$  and  $C_1$  were found by observing the diffusion voltage across the RC pair of the cells during charging. The parameters were chosen to fit the exponential behaviour of individual cells and charging protocols in the training set and an average was taken for the final values which are given in Table 1.

The  $OCV(z(t))$  function fitting the training set was derived using the  $v_{out}$  data, parameter values and  $OCV(z(t)) = v_{out}(t) - v_1(t) - R_0i(t)$ . The parameter values and the OCV function are needed for derivation of one another and so the model training was done iteratively until the model performance on the training set was deemed satisfactory. For the optimisation problem, the  $OCV$  function was a piecewise polynomial, as defined in Appendix C.

#### 2.4.2. Estimating the thermal model parameters

Only batch 5 of the data-set from [36] includes temperature data. Batch 5 includes 45 cells, containing 9 unique charging protocols with 5 cells cycled with each protocol [36]. As with the electrical model only the first cycle of the ‘new’ cell was considered for training and testing. In the ‘read me’ attached to the data of [36] it was stated that the temperature data was unreliable and that the thermocouples sometimes lost contact during cycling. Samples with anomalously low temperature increases over charging were removed from the data set, along with those with missing data points over long periods of time. There were only 27 cell charging samples remaining after cleaning the data in this way, and this included 8 unique charging protocols. The training set consisted of 13 randomly selected cells from the cleaned batch 5, and the testing set consisted of the remaining 14. The training set contained 7 unique protocols; the testing set also contained 7 unique protocols, 6 of which were present in both sets with one charging protocol unique to each set.

The temperature data in the dataset often showed a sizeable difference between the starting and ambient temperature readings and was notably noisy. The cells in this batch were cycled at the same time in a forced convection temperature chamber set to 30°C [36], so it was expected that the ambient temperature would be the same and equal to 30°C across the data. This was found not to be the case and it was decided to trust the temperature reading of the forced convection chamber over the thermocouples. Accordingly, the remaining data were shifted so that the initial temperature data point was equal to 30°C in all cases. In the model,  $T_{amb} = 30^\circ\text{C}$  and was assumed to not change with time.

The model parameters of  $m$  and  $A$  were estimated using the cell datasheet [49] and  $c_p$  and  $h$  were estimated using the RANSAC (Random Sample Consensus) procedure [50]. Within this procedure, the MATLAB ODE fitter `greyest` [51], which provides optimal model parameters for individual input/output samples, was used. Here, `greyest` was configured to take the temperature and power generated from the data of [36] as inputs and produce estimates for  $h$  and  $c_p$  that minimised the mean square error between the temperature data and the simulated temperature, computed using Equation (7), for each sample in the training set. The data used was from the first 1500s of the cycle which included the vast majority of the cell charging time. `greyest` was applied to all samples in the training set, generating a different candidate model for every sample. These candidate models were then used to predict the cell temperature during charging for every sample in the training set. The candidate model with the lowest average mean square error across the training set was then selected. The parameters found by this method are given in Table 1. As the thermal model uses the electrical model as an input the identification of the thermal parameters is dependent on the electrical parameters, as shown in Equation (7).

#### 2.4.3. Model performance

Table 2 shows a comparison of the error statistics for the electrical model for both the training set (batch 1), and the testing set (batch 5 with repetitions and matches with the training set removed). The mean square error (MSE) between the experimental and simulated voltages shown was calculated for each cell in the dataset over the the first 10 minutes of charging, as this was the critical region for the optimisation. The error was calculated between samples taken every 0.01 s.

Parameter	Value	Units
Electrical model		
$R_0$	0.0163	$\Omega$
$R_1$	0.0221	$\Omega$
$C_1$	678.733	F
$Q$	3960	As
Thermal model		
$m$	$39 \times 10^{-3}$	kg
$A$	$3.714 \times 10^{-3}$	$m^2$
$c_p$	2025.737	$Jkg^{-1}K^{-1}$
$h$	43.061	$Wm^{-2}K^{-1}$
Experimental protocol		
$p$	0.2	
$K$	4	

Table 1: Estimated parameters for the cell electrical and thermal models.

Dataset	Median MSE (mV) <sup>2</sup>	Mean MSE (mV) <sup>2</sup>	MSE SD (mV) <sup>2</sup>
Training Set	195.0	225.3	126.7
Testing Set	748.2	737.8	211.6

Table 2: Table displaying the median, mean and standard deviation (SD) of the mean square error (MSE) of the simulated voltage response upon charging up to 80% SOC ( $t_{max} = 600$  s) compared against the data of [36].

Figures 2 and 3 show the performance of the electrical model over the whole charging cycle against examples from the testing and training set respectively. Figure 3 shows the worst performance of the model, over the first 600 s of charging, against a charging protocol in the testing set.

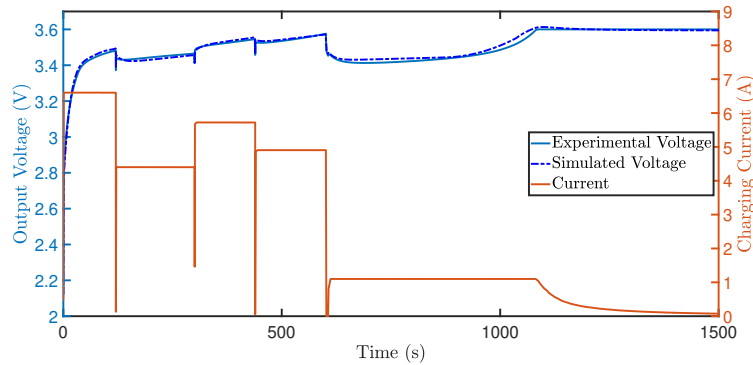


Figure 2: Electrical model output compared to a protocol on the training set, mean squared error of 176.094 (mV)<sup>2</sup>.

The error from the voltage model was low during the first 80% of charging, but small errors in the model may have led to errors in the optimisation. Figure 3 shows the sample with the largest error over the first 10 minutes which was still deemed acceptable.

Figures 2 and 3 both display a characteristic present throughout the dataset where there are drops in current, and therefore in voltage, prior to the step changes in current. This led to similar drops in calculated heat generated shown in Figures 4 and 5.

The performance of the thermal model is given in Table 3. Due to a number of anomalous samples with large error the mean is skewed by the presence of these anomalous samples, so the median MSE is also given. Figure 4 shows

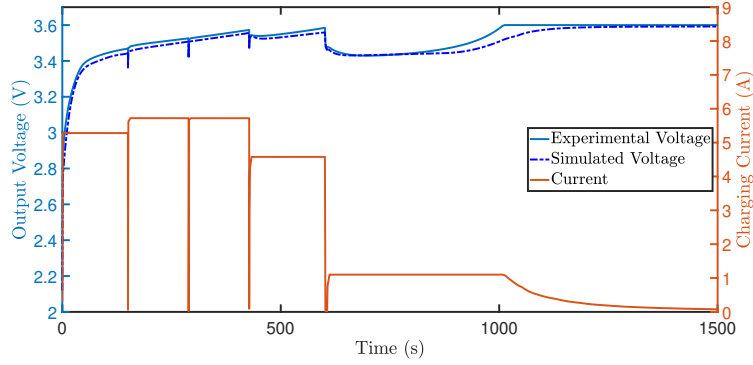


Figure 3: Electrical model performance on the protocol in the testing set with the greatest error over the first 10 minutes of charging, mean squared error of  $1070.546 \text{ (mV)}^2$ .

the performance of the thermal model on the cell from the training set with the median error, and Figure 5 shows the performance of the thermal model on a cell from the testing set with a larger error.

Dataset	Median MSE ( $\text{K}^2$ )	Mean MSE ( $\text{K}^2$ )	MSE SD ( $\text{K}^2$ )
Training Set	0.2260	0.3802	0.4178
Testing Set	0.3025	0.7617	1.0784

Table 3: Table displaying the median, mean and standard deviation (SD) of the mean square error (MSE) of the simulated thermal response upon charging up to 80% SOC ( $t_{max} = 600 \text{ s}$ ) compared against the data of [36].

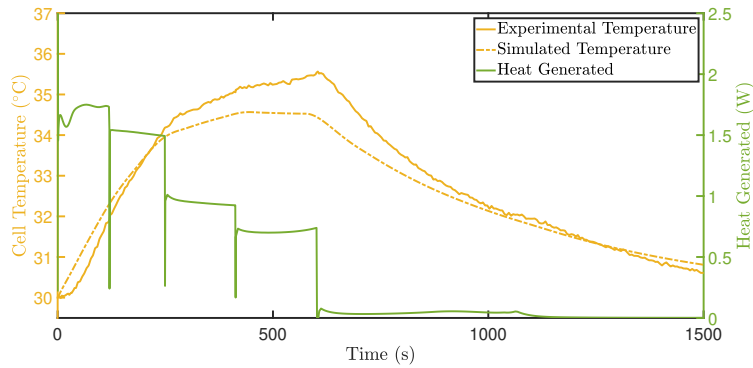


Figure 4: Thermal model performance on a cell from the training set. Mean squared error of  $0.2260 \text{ K}^2$ .

The performance of the thermal model is not to the same standard as the electrical model. As shown by Figures 4 and 5, the model often underestimates the peak temperature of the cell. Table 3 shows the standard deviation of the error is large in both the training set and in the testing set which is likely due to the issues with the thermal training dataset described above. Using the thermal model with the voltage model as its input will introduce more error, however, it is likely that the error will still be dominated by the thermal model. These errors are unlikely to have affected the general behaviour of the model and the conclusions of this report.

### 3. Generating the fast charging protocols

The discrete model in (10) was used to find optimal current charging profiles to maximise the number of cycles to failure whilst charging the cells to 80% SOC in 10 minutes. The underlying motivation of the proposed approach was

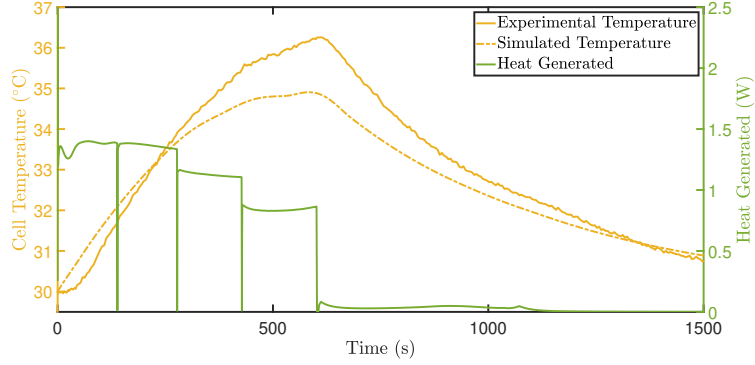


Figure 5: Thermal model performance on a cell from the testing set. Mean squared error of 0.4223 K<sup>2</sup>.

to interpret the cycle-life predictor of [36] in terms of physical quantities, i.e. the evolution of the model's states, so that it could be used within a model-based control problem and then be optimised.

The greatest challenge in solving this problem was defining the objective function associated with the optimal charging profiles given in [36] which maximised cycles to failure. Two objective functions are presented, one which was found from the data of [36] using linear regression and the second minimised the cumulative increase in cell temperature during the charge.

### 3.1. Problem set-up

The optimal charging profiles were generated by solving optimisation problems of the form

$$\min_{\mathbf{x}} f(\mathbf{x}) \quad (16a)$$

$$\text{subject to: } \begin{cases} c(\mathbf{x}) \leq \mathbf{0}, \\ c_{eq}(\mathbf{x}) = \mathbf{0}, \\ \mathbf{P}\mathbf{x} \leq \mathbf{q}. \end{cases} \quad (16b)$$

Here, the cost function is denoted by  $f(\mathbf{x})$ , the nonlinear equality constraints of the problem are captured by the vector  $c_{eq}(\mathbf{x})$ , the nonlinear inequality constraints by  $c(\mathbf{x})$  and the linear inequality constraints by  $\mathbf{P}\mathbf{x} \leq \mathbf{q}$ . This separation between nonlinear and linear inequality constraints was made just to clarify the problem formulation. The decision vector  $\mathbf{x}$  was formed from the state and applied current values at each time step, where  $K = 4$  is the total number of time-steps

$$\mathbf{x} = [i[0], v_1[1], z[1], \Delta T[1], i[1], v_1[2], z[2], \Delta T[2], \dots, i[K-1], v_1[K], z[K], \Delta T[K]]^T. \quad (17)$$

It was assumed that each cell was initially completely discharged and  $v_1[0] = z[0] = \Delta T[0] = 0$  and that charging ceased immediately after  $K$  steps, so  $i[K] = 0$  A. The time steps were defined such that the cell was charged an equal amount of SOC in each time step, in this work and in [36] this was 20% SOC per step.

### 3.2. Constraints

The equality constraints of (16b) ( $c_{eq}(\mathbf{x}) = \mathbf{0}$ ) were used to include the cell model and the problem definition in the optimisation. Thus, the rows of  $c_{eq}(\mathbf{x})$  implemented the discrete cell model (10) and ensured the sum of the variable time steps equalled 10 minutes. The definition of  $\Delta t[k]$  (12) ensured SOC = 80% after 10 minutes if  $K = 4$  and  $p = 0.2$ .

The inequality constraints of (16b) ( $c(\mathbf{x}) \leq \mathbf{0}$  and  $\mathbf{P}\mathbf{x} \leq \mathbf{q}$ ) were used to impose bounds on the states of the model. Upper and lower limits were imposed on  $i$ ,  $z$ , and  $\Delta T$  using the linear inequality constraint,  $\mathbf{P}\mathbf{x} \leq \mathbf{q}$ . The matrix  $\mathbf{P}$  is a sparse selector matrix where each row contains a single 1 or -1 to select an element of  $\mathbf{x}$  and  $\mathbf{q}$  is a column vector.

These elements were defined by the following inequalities

$$-i[k] \leq -i_{min}, \quad \forall k \in [0, K-1], \quad (18)$$

$$z[k] \leq z_{max}, \quad \forall k \in [1, K], \quad (19)$$

$$-z[k] \leq -z_{min}, \quad \forall k \in [1, K], \quad (20)$$

$$\Delta T[k] \leq \Delta T_{max}, \quad \forall k \in [1, K]. \quad (21)$$

Here,  $z_{max} = 1$  and  $z_{min} = 0$  (from the definition of SOC [48]), and  $i_{min} = 0$  A (only charging, no discharging). The maximum current input was indirectly limited by the bounds on voltage and temperature, which is consistent with the bounds set in [36]. The maximum allowable increase in temperature  $\Delta T_{max}$  was  $4.5^\circ\text{C}$ , as this was the maximum observed temperature increase seen in our simulations of the top three performing charging currents from [36], which all reached  $\approx 34.5^\circ\text{C}$  after 10 minutes and the first 4 current steps.

The nonlinear inequality constraints were defined by the upper and lower bounds on output voltage. Thus, the rows of the output vector of  $c(\mathbf{x})$  are equal to the following expressions

$$v_{out}[k] - v_{max}, \quad \forall k \in [0, K], \quad (22)$$

$$-v_{out}[k] + v_{min}, \quad \forall k \in [0, K], \quad (23)$$

$$v_{out}[k - \delta t] - v_{max}, \quad \forall k \in [1, K], \quad (24)$$

$$-v_{out}[k - \delta t] + v_{min}, \quad \forall k \in [1, K], \quad (25)$$

where  $v_{max} = 3.6$  V and  $v_{min} = 0$  V to be consistent with [36]. Without the additional constraint on  $v_{out}[k - \delta t]$ , the voltage just before the switching point of the currents was found to exceed the bound during the fast charging, as a result of the  $R_0 i[k]$  term. Imposing this additional constraint prevented this violation.

### 3.3. Cost function

The cost function  $f(\mathbf{x})$  was designed to minimise cell degradation during a fast charge to 80% SOC in 10 minutes. The first approach for designing the cost function, which is a key concept in this paper, was to learn its structure directly from the data of the four-step charging protocols from [36] and relate this learned function back to the identified model's states. Battery degradation is generally regarded as being challenging to model accurately and efficiently, as it comprises a complex combination of inter-related physical and chemical mechanisms [52, 38, 53]. For example, one of the dominant mechanisms for cell degradation is the growth of the 'solid electrolyte interphase' (SEI) [52]. Generally, a greater temperature during (dis)charging leads to a greater rate of SEI layer growth and degradation [54], which would suggest that high temperatures are detrimental to the health of the cell. Conversely, lithium plating, another degradation mechanism that is particularly prevalent during fast charging, causes greater battery degradation at lower temperatures [55]. So, exposure to both high and low temperatures can be detrimental to a battery's health. Together, such mechanisms highlight the difficulty in defining an all encompassing cost function to represent battery degradation in terms of a models' physical states. For this reason, that there has been significant interest in the use of data-driven methods to compute fast charging protocols, such as those used in [36, 38].

The results of this paper build on those from [36], where fast charging protocols were generated using a data-driven approach to maximise the number of cycles to failure. As in [36], we define 'cycles-to-failure' ( $CtF(\mathbf{x})$ ) as the number of cycles prior to the discharge capacity of the cell dropping below 80%. In this paper, the goal was to obtain an expression for this predictor in terms of the evolution of the model states and applied currents of (10). In other words, the goal was to open the black box of the cycle-life predictor from [36], giving it a physical interpretation and enabling it to be used within a model-based optimal control problem.

To this end, the cycles-to-failure were expressed as

$$CtF(\mathbf{x}) = w_1 i[0] + w_2 i[1] + w_3 i[2] + w_4 i[3] + w_5 \Delta T[1] + w_6 \Delta T[2] + w_7 \Delta T[3] + w_8 \Delta T[4] + w_9, \quad (26)$$

which is a weighted sum (with weights  $\mathbf{w}$ ) of the applied current and temperature values at each sampling point during the fast charge. To estimate the weight vector  $\mathbf{w}$ , batch 5 of [36] was used, as it was the only batch with known cycles to failure. As batch 5 only contained nine unique charging protocols, the weight vector  $\mathbf{w}$  could only contain nine

elements if all protocols were to be used for training, in order to avoid issues of over-fitting. The structure of (26) contains the current and temperature information at each of the discrete steps. This simple linear function is only a heuristic, with this parameterisation chosen to capture the complex relationship between degradation rates and cell temperature as well lithium plating and the charging current. If more data was available, then more general features would have been used in (26), including voltage information.

This limitation reinforces the need for more training data, composed of various different cell charging profiles and cells, if the full extent of these battery management and control methods are to be exploited.

The state samples ( $\mathbf{x}$ ) used to generate the weights were obtained from the variable-time-step model (Equation (10)) rather than the raw data, as this ensured consistency throughout the training data for the  $CtF$  model of Equation (26). The weight vector  $\mathbf{w}$  for the  $CtF(\mathbf{x})$  was then found using standard least-squares fitting

$$\mathbf{w} = (\Lambda^\top \Lambda)^{-1} \Lambda^\top \mathbf{b}$$

where  $\Lambda$  is a  $(45 \times 9)$  matrix with rows of the simulated states ( $\mathbf{x}$ ) corresponding to the coefficients of the elements of  $\mathbf{w}$  in Equation (26), and  $\mathbf{b}$  is a  $(45 \times 1)$  column vector containing the experimental cycles to failure of each of the nine unique charging protocols' five repetitions.  $w_6$  was found to be negative, whereas  $w_5$ ,  $w_7$ , and  $w_8$  were found to be positive, suggesting that a high  $\Delta T[k]$  is beneficial to cycle life at some time instants and not at others. Such details further highlight the complexities of correctly capturing degradation features within a single, state-defined, cost function. The trained elements of  $\mathbf{w}$  are given in Appendix D.

Because the rank of  $\Lambda$  is equal to the number of weights, the predictions for each of the nine training protocols are equivalent to the mean of their five experimental cycles to failure. The mean absolute error between the predicted and experimental cycles to failure across the training set was 76.5 cycles, which is due to variation in the experiments from their corresponding experimental mean. It is noted that this is not best practice and the performance of the model when extrapolating outside of the trained range is not expected to be good. This also meant that there was not enough data for a testing set so the performance of this model could not be validated. However, this was considered the best course of action given the limited availability of open-source experimental cycling data in [36].

As well as cycles-to-failure, another cost function was considered, the cumulative gain in cell temperature during the fast charge

$$T_\Sigma(\mathbf{x}) = \sum_{j=1}^K \Delta T[j]. \quad (27)$$

The reason for including this additional cost function in the results was to highlight the flexibility of the model-based optimisation to adapt to new problem settings. This cost function was identified after it was noticed that the temperature plots of cells charged with the optimal profiles from [36] all appeared to have a low integral of temperature.

### 3.4. Solution method

The MATLAB function `fmincon` [56] was used to solve the optimisation problems of Equation (16). It was found that, primarily due to the time-varying step-sizes of Equation (12), the optimisation problem of Equation (16) was non-convex. For that reason, local optima were obtained when the optimisation was initialised at different starting conditions, corresponding to the currents being uniformly distributed as random values between 0 and 10 A and the all other states initialised at 0. Here, 5000 such randomly sampled initial conditions were considered. Generally, the computed local minima found were expected to be close to the global minimum, as the local minima did not show significant variation. The solution giving the lowest cost function value was then taken as the global minima. It is acknowledged that more advanced optimisation solvers than `fmincon` exist for solving such problems, but this algorithm was found to be sufficient for the problem at hand. Notably, it was easy to implement (especially in handling the constraints of (16b)), scalable and provided good solutions. From inspection of the local minima, it is not expected that significant reductions in the cost would be achievable using more advanced algorithms specifically designed for non-convex problems.

## 4. Results

This section details the results obtained from implementing the above fast charging optimisation method. Figures 6 and 7 show current profiles and corresponding outputs which maximised the predicted cycles to failure with  $f(\mathbf{x}) = -CtF(\mathbf{x})$ .

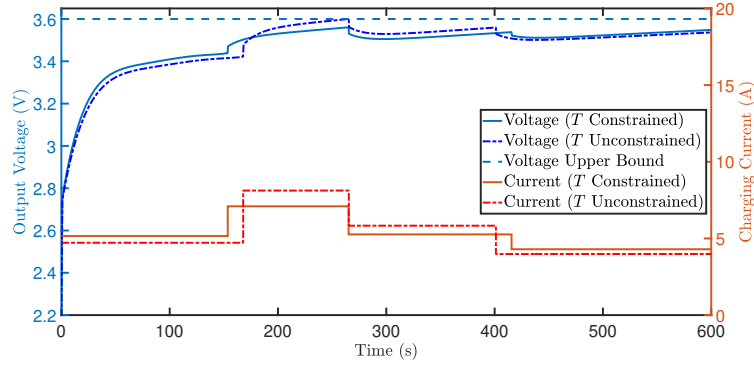


Figure 6: The optimal charging profiles to maximise cycle life whilst charging a cell to 80% SOC in 10 minutes, and the voltage response of these current inputs. Solutions for when both the temperature is constrained and when it is unconstrained are shown.

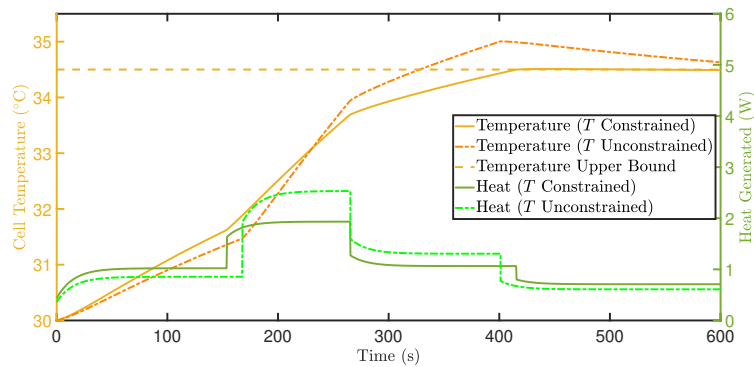


Figure 7: The cell thermal responses and heat generation rates to the charging profiles of Figure 6.

In these figures, the impact of applying the constraint of Equation (21) limiting the increase in cell temperature was also investigated. It was found that when the temperature constraint was in place, the optimal solution predicted the number of cycles-to-failure would be 978 cycles, but when the temperature constraint was removed, it predicted 1078 cycles. Both of these values exceeded all of the cycle-to-failure predictions made by the model (26) for charging protocols in its training set, highlighting the benefits of model-based optimisation.

For reference, the experimental minimum, maximum, and mean cycle lives from the validation batch of the top three optimal charging profiles from [36] are given in Table 4 along with the cycle lives predicted by the ‘early outcome predictor’ of [36]. Using the labelling notation of [36], the computed optimal protocol obtained by solving Equation (16) with the temperature constraint was (4.688C-6.451C-4.786C-3.905C) and without the temperature constraint it was (4.289C-7.384C-5.301C-3.621C). In this notation the current of each of the four steps are given in order in C-rate.

### 4.1. Discussion

With only limited available data to train the linear model for the cycles-to-failure of Equation (26), care should be taken when extrapolating the predictions for the cycles-to-failure of this model. The estimations from the experiments of [36] and their early outcome predictor should be regarded as being more trustworthy, although consideration of

Charging Profile	Mean Cycle Life	Minimum Cycle Life	Maximum Cycle Life	Early Outcome Predictor [36]	Model Predicted Cycle Life (26)
CLO1 (4.8C-5.2C-5.2C-4.160C)	890	774	1082	1185	890
CLO2 (5.2C-5.2C-4.8C-4.160C)	912	775	1166	1183	912
CLO3 (4.4C-5.6C-5.2C-4.252C)	884	678	1089	1174	884
Maximising $CtF$ ( $\Delta T_{max} = 34.5^\circ\text{C}$ )					978
Maximising $CtF$					1078
Minimising $\sum_{j=1}^K \Delta T[j]$ ( $\Delta T_{max} = 34.5^\circ\text{C}$ )					670

Table 4: Table comparing the experimental cycle lives and cycle lives predicted by the early outcome predictor of [36], as well as the predictions of Equation (26). CLO1-3 were present in the training set of the  $CtF$  model so predictions are equivalent to the mean cycle life. Protocols are denoted by (CC1-CC2-CC3-CC4) in C-rate.

Table 4 shows even that predictor is fallible and that experimental cycle lives can vary over a range of hundreds of cycles. Any optimal profile that is estimated to have a cycle life greater than its training set should be treated with caution until further experiments are carried out, since it is extrapolating beyond its training data. Therefore, it is acknowledged that the proposed optimal charging protocols should be validated against other suggested optimal profiles and the rest of the validation set of [36]; a greater number of trials of each protocol will be required to be confident in its mean predicted cycle life.

The cycle life model of (26) could have been trained from the early outcome predictions for each of the 224 charging profiles trialled by [36] for a larger training dataset. However, all of the predictions have large predicted standard deviations of roughly 100 cycles [36] and training a model on these predictions would introduce the same biases into our model. It would then be unsurprising if the model predicted the same or a similar charging profile to the protocol with greatest predicted cycle life from [36] (CLO1) as one which would maximise cell cycle life. The same argument could be made based on the fact that the top three protocols of [36] (CLO1-3) were in batch 5 which was used to train the cycle life predictor model (26) and constituted the protocols with the largest cycle life; consequently, it may be possible that the proposed approach is also biased in their favour.

With the proposed method involving a model-based optimisation, there is a continuous parameter space of current steps to explore. This continuous search space contrasts with the discrete steps allowed in the experiments of [36] which yielded 224 set different current profiles to experiment on. The discrete levels allowed for CC1-3 were spaced every 0.4C between 3.6C and 6C [36]. Of the discrete profiles considered in [36], the 4-step protocols ‘closest’ to the computed optimal solution of Equation (16) with  $\Delta T_{max} = 34.5^\circ\text{C}$  were: (4.4C-6C-4.8C-4.328C) which was ranked #27/224 with a predicted cycle life of 1120, and (4.8C-6C-4.8C-4C) which was ranked #36/224 with a predicted cycle life of 1104 (cycle lives predicted by [36]). The protocol closest to the optimal solution of Equation (16) without the upper bound on temperature was (4.4C-7C-5.2C-3.691C), which was ranked #61/224 with a predicted cycle life of 1022. Given the large experimental range of cycle lives of the protocols in the data and the standard deviation of the predicted cycle lives being around 100 for each protocol, it is expected that the protocols generated by solving Equation (16) would have cycle lives comparable, or better, than the best performing ones of [36] because of the model-based optimisation.

The objective function minimising the sum of the sampled cell temperature values (given by  $T_\Sigma(\mathbf{x})$  in Equation (27) and subject to the thermal constraint of Equation (21)) was also trialled as a candidate function for which the optimal profiles from [36] were minimising. Figures 8, 9, and 10 show comparisons of current, voltage, and temperature between the top 3 protocols from [36] (CLO1-3), the 4-step current profile which minimised the sum of the sampled temperatures, and the protocol which maximised the cycle life of Equation (26) subject to the temperature constraint of Equation (21). Each of these protocols were simulated using the discrete model of Equation (10) at a time step of  $\Delta t[k] = 0.001$  s. The figures show that this objective function of the sum of the sampled temperatures

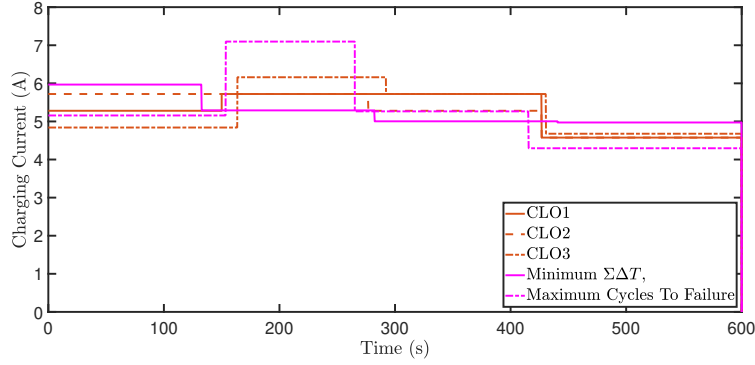


Figure 8: Comparison of the optimal current profiles of [36] compared to our optima for minimising the sum of sampled temperatures and maximising predicted cycle life.

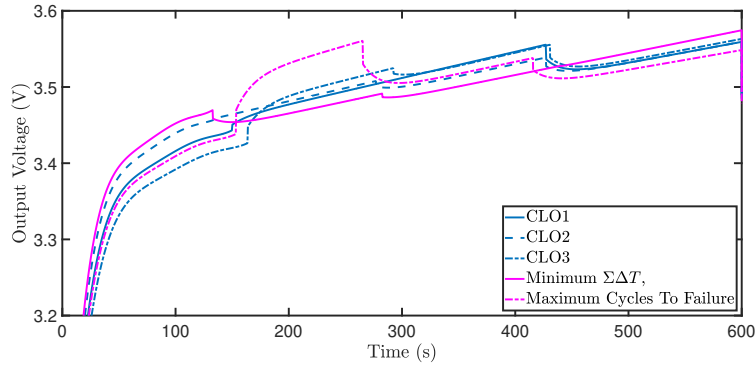


Figure 9: Comparison of the optimal voltage profiles of [36] compared to our optima for minimising the sum of sampled temperatures and maximising predicted cycle life.

performed well given its simplicity. The optimum charging profile it generated was more similar to the best performing profiles of [36] than the protocol which maximised the cycles-to-failure of (26). However, having similar profiles did not relate to similar predicted cycles-to-failure. As Table 4 shows, the  $CtF$  for the protocol minimising the sum of the temperatures was 670 which was significantly lower than the  $CtF$  of 890 for CLO1. This difference highlights the sensitivity of a cell’s cycles-to-failure with respect to the cycling protocol and how even similarly looking protocols can have significant variations in their cycle lives. It also highlights the benefits of optimising over the learned cost function, by maximising the  $CtF$  directly, compared to using adhoc descriptions of cell degradation such as the sum of temperatures.

In order for methods such as the model-based solution of Equation (16) to be used effectively, an accurate cell model was required as well as a suitable definition of the cost function (e.g. minimising cell degradation). For maximising cell cycle life, the objective function was difficult to define [52, 38, 53], particularly since only the first cycle was simulated. In [36], data from the first 100 cycles were used and despite this, the cycles-to-failure predictor still over-predicted the cycle lives of its top three optimal charging protocols, often by over 100 cycles [36]. Ultimately, it is difficult to model and optimise for cycles-to-failure when the number of cycles can change by 100 between experiments using the same charging protocol [36]. In order to train models for degradation estimation, more data is required and data-driven methods will have to be employed in tandem with models.

## 5. Conclusions

In this paper, a method to optimise fast charging profiles for lithium ion batteries was proposed. The main novelty of the proposed method was its “*hybrid*” nature, combining elements of both data-driven and model-based algorithms

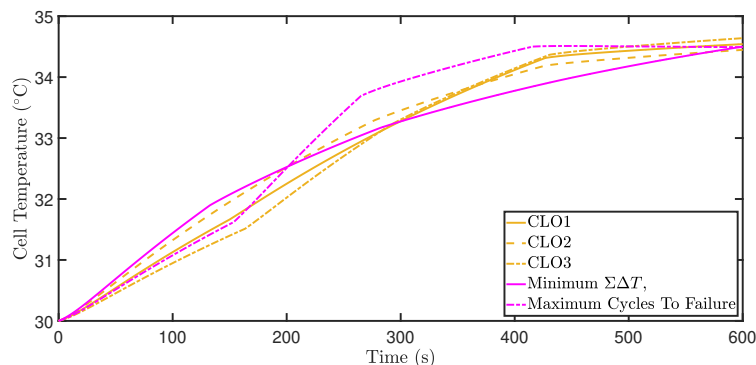


Figure 10: Comparison of the optimal temperature profiles of [36] compared to our optima for minimising the sum of sampled temperatures and maximising predicted cycle life.

to compensate for each of their weaknesses and exploit their strengths. In particular, the proposed method interpreted the fast charging protocols of [36], obtained using a data-driven approach, as the solution of a model-based optimal control problem. This problem formulation gave the method extra flexibility, in the sense that it exploited the ability of the data-driven approach to learn cell degradation directly from the data with the model-based approach’s strengths of extrapolation, optimisation and providing performance guarantees. Extended use of this method is likely to lead to time and computational efficiency gains, meaning that optimised charging protocols are found that are better than those determined using a purely data-driven approach and are identified with fewer experiments. The advantages of the proposed approach were demonstrated by computing fast charging profiles for A123 Systems APR18650M1A cells, the results of which predicted an increase in the cycles-to-failure from 912 to 1078 cycles compared to [36]. Such performance gains highlight the potential of fusing data-driven and model-based algorithms for optimising fast charging protocols. Retraining the model and re-applying the method after a set amount of cycles would allow the optimised fast charging currents to adapt in response to the cell ageing. The work-flow outlined in Figure E.13 of Appendix E details how such adaptive charging could be implemented.

The results of this paper identified several opportunities for future work. Most importantly, the need for rich, large, open-source data sets of lithium ion batteries, covering a range of different charging profiles and chemistries, was highlighted as a critical bottleneck for the development of fast charging algorithms. Moreover, even though significant performance gains were predicted using the proposed method that was based upon simple models, further gains are to be expected with more comprehensive models and algorithms, for example electrochemical models. The value of using electrochemical models is that the degradation mechanisms could be included directly into the fast charging optimal control problem, rather than being learned from data. However, existing models for battery degradation are challenging to parameterise and there has been relatively limited degradation model validation against experimental data– which is why data-driven solutions have grown in recent years. Finally, there are potential benefits from synchronising the model development and data-collection steps of the process highlighted. Here, the model was developed after the experiments were conducted; in fact, they were trained on the data of [36]. If the model development had instead been conducted as the data was collected then it could have been used to propose new testing protocols, thereby potentially reducing the number of experiments required and increasing the richness of the data sets. Combining the modelling and data collection work at the earliest stages of lithium ion battery research projects is expected to produce the greatest benefits, as opposed to retrofitting models onto historical data.

## Acknowledgements

Ross Drummond was supported by a UK Intelligence Community Research Fellowship from the Royal Academy of Engineering. Stephen Duncan was supported by the Nextrode project, funded by the UK Faraday Institution [grant number FIRG015].

## Appendix A. $R_0$ variation with SOC

Values of  $R_0$  were calculated from the training set at different values of SOC. In [36], the charging protocols contained step changes in the charging current every 20% SOC which allowed the estimation of the series resistance  $R_0$  at these points by dividing the magnitude of the step change in voltage by the corresponding magnitude of the step change in current [48]. It was found that the value of  $R_0$  was approximately constant across values other than at SOC = 0, where it was higher. This is shown in Figure A.11. Different schemes were trialled with a higher  $R_0$  at low SOC, but all caused an initial overshoot of  $V_{out}$  unless  $R_0$  fell to its steady state value almost instantaneously, to the point where taking  $R_0$  to be constant was an acceptable simplification; any error this introduced would be absorbed into an artificial increase in  $OCV(z)$  at low SOC. Whilst this may not be reflective of experimental data [41] this gave the advantage of a simpler model and faster optimisation. The constant value of  $R_0 = 0.0163\Omega$  used is the average value of the data points for  $R_0$  excluding the values when  $z = 0$ .

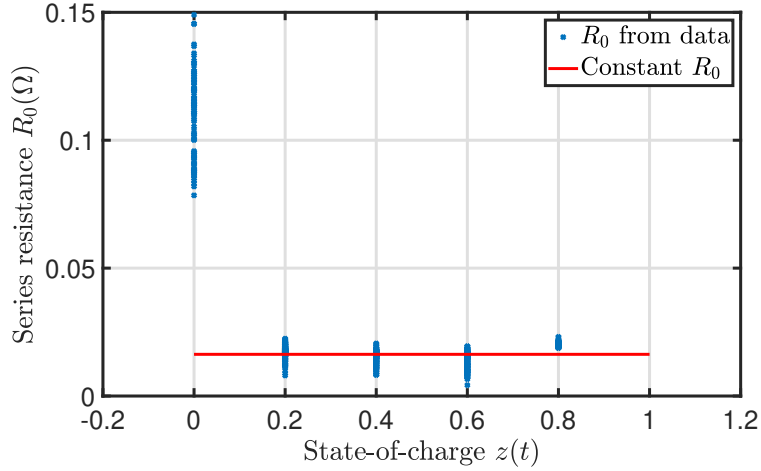


Figure A.11: Variation of  $R_0$  with SOC estimated from the data of [36].

## Appendix B. Derivation of the discrete time model

To pose the optimisation as a discrete-time optimal control problem, it was necessary to discretise this model in time with the states being defined along the sampling points  $t_k$ ,  $k = 0, 1, \dots, K$ . Square brackets will be used to denote the discrete-time signals throughout, as in  $i[k] = i(t_k)$  with the sampling interval  $\Delta t_k$  between times  $t_{k-1}$  and  $t_k$  described by Equation (12).

During the discretisation, the current  $i(t)$  satisfied a zero-order hold profile, changing only at the sampling points  $t_k$ . This resulted in a discrete-time current sequence defined by  $i[k] = i(k\Delta t[k] + \delta t) \quad \forall \delta t : 0 \leq \delta t < \Delta t[k]$ .

The goal was then to integrate the continuous dynamics of Equations (1) and (7) across one time-step to generate the discrete time model. Beginning with the electrical dynamics, and with the current  $i[k]$  being zero-order hold, the discretised relaxation voltage from Equation (1) was simply

$$v_1[k+1] = e^{-\lambda_1 \Delta t[k]} v_1[k] + b_1 i[k] \int_{t_k}^{t_{k+1}} e^{-\lambda_1 (t_{k+1} - \tau)} d\tau, \quad (\text{B.1})$$

$$= e^{-\lambda_1 \Delta t[k]} v_1[k] + \frac{b_1}{\lambda_1} (1 - e^{-\lambda_1 \Delta t[k]}) i[k]. \quad (\text{B.2})$$

Similarly, the discretised state-of-charge was

$$z[k+1] = z[k] + b_2 i[k] \int_{t_k}^{t_{k+1}} d\tau = z[k] + b_2 i[k] \Delta t[k]. \quad (\text{B.3})$$

However, obtaining an exact expression for the discretised thermal model equation is complicated by the  $v_1(t)i(t)$  term in Equation (9). Whilst  $i(t)$  is constant over the sampling period,  $v_1(t)$  is not, and, therefore, neither is  $v_1(t)i(t)$ . By integrating the thermal dynamics of (7), then

$$\begin{aligned}\Delta T[k+1] &= e^{-\lambda_2 \Delta t[k]} \Delta T[k] + \int_{t_k}^{t_{k+1}} e^{-\lambda_2(t_{k+1}-\tau)} (b_3 i[k]^2 + b_4 v_1(\tau) i[k]) d\tau, \\ &= e^{-\lambda_2 \Delta t[k]} \Delta T[k] + \frac{b_3}{\lambda_2} (1 - e^{-\lambda_2 \Delta t[k]}) i[k]^2 + b_4 i[k] \int_{t_k}^{t_{k+1}} e^{-\lambda_2(t_{k+1}-\tau)} v_1(\tau) d\tau.\end{aligned}$$

Using Equation (B.2), the relaxation voltage ( $v_1(t)$ ) during the sampling period can be shown to satisfy

$$v_1(t) = e^{-\lambda_1(t-t_k)} v_1[k] + \frac{b_1}{\lambda_1} (1 - e^{-\lambda_1(t-t_k)}) i[k], \quad \forall t \in [t_k, t_{k+1}]. \quad (\text{B.4})$$

Substituting this expression into Equation (B.4) allows the integral of Equation (B.4) to be calculated exactly, as detailed in Equation (B.5). Substituting this expression back into Equation (B.4) gives the exact form of the discrete-time thermal dynamics, given in Equation (B.9).

$$\int_{t_k}^{t_{k+1}} e^{-\lambda_2(t_{k+1}-\tau)} v_1(\tau) d\tau = \int_{t_k}^{t_{k+1}} e^{-\lambda_2(t_{k+1}-\tau)} \left( e^{-\lambda_1(\tau-t_k)} v_1[k] + \frac{b_1}{\lambda_1} (1 - e^{-\lambda_1(\tau-t_k)}) i[k] \right) d\tau, \quad (\text{B.5})$$

$$= v_1[k] \int_{t_k}^{t_{k+1}} e^{-\lambda_2 t_{k+1} + \lambda_1 t_k + (\lambda_2 - \lambda_1)\tau} d\tau + \frac{b_1}{\lambda_1} i[k] \int_{t_k}^{t_{k+1}} (e^{-\lambda_2 t_{k+1} + \lambda_2 \tau} - e^{-\lambda_2 t_{k+1} + \lambda_1 t_k + (\lambda_2 - \lambda_1)\tau}) d\tau, \quad (\text{B.6})$$

$$\begin{aligned}&= \frac{1}{\lambda_2 - \lambda_1} (e^{-\lambda_1 \Delta t[k]} - e^{-\lambda_2 \Delta t[k]}) v_1[k] \\ &\quad + \frac{b_1}{\lambda_1 \lambda_2} (1 - e^{-\lambda_2 \Delta t[k]}) i[k] - \frac{b_1}{\lambda_1 (\lambda_2 - \lambda_1)} (e^{-\lambda_1 \Delta t[k]} - e^{-\lambda_2 \Delta t[k]}) i[k].\end{aligned} \quad (\text{B.7})$$

$$\begin{aligned}\Delta T[k+1] &= e^{-\lambda_2 \Delta t[k]} \Delta T[k] + \frac{b_3}{\lambda_2} (1 - e^{-\lambda_2 \Delta t[k]}) i[k]^2 + \frac{b_4}{\lambda_2 - \lambda_1} (e^{-\lambda_1 \Delta t[k]} - e^{-\lambda_2 \Delta t[k]}) i[k] v_1[k] \\ &\quad + \frac{b_1 b_4}{\lambda_1 \lambda_2} (1 - e^{-\lambda_2 \Delta t[k]}) i[k]^2 - \frac{b_1 b_4}{\lambda_1 (\lambda_2 - \lambda_1)} (e^{-\lambda_1 \Delta t[k]} - e^{-\lambda_2 \Delta t[k]}) i[k]^2,\end{aligned} \quad (\text{B.8})$$

$$\begin{aligned}&= e^{-\lambda_2 \Delta t[k]} \Delta T[k] \\ &\quad + \left( \left( \frac{b_3}{\lambda_2} + \frac{b_1 b_4}{\lambda_1 \lambda_2} \right) (1 - e^{-\lambda_2 \Delta t[k]}) - \frac{b_1 b_4}{\lambda_1 (\lambda_2 - \lambda_1)} (e^{-\lambda_1 \Delta t[k]} - e^{-\lambda_2 \Delta t[k]}) \right) i[k]^2 \\ &\quad + \frac{b_4}{\lambda_2 - \lambda_1} (e^{-\lambda_1 \Delta t[k]} - e^{-\lambda_2 \Delta t[k]}) i[k] v_1[k].\end{aligned} \quad (\text{B.9})$$

Collecting Equations (B.2), (B.3), and (B.9) gives the full discrete state space model of Equation (10) with the parameters defined in Equation (11).

### Appendix C. Piece-wise polynomial OCV curve

Using the parameters of Table C.5, the open circuit voltage  $OCV(z(t))$  curve was fitted using the piece-wise polynomial

$$OCV(z(t)) = \sum_{j=0}^5 \omega_{i,j} (z(t) - Z_{i-1})^j, \quad \forall z(t) \in [Z_{i-1}, Z_i] \quad (C.1)$$

with the weights  $\omega_{i,j}$  and the local regions of the piece-wise polynomial approximation  $Z_i$  stated in Table C.5 . Here, the total number of regions was  $i = 1, 2, \dots, 6$  and  $Z_0 = 0$ .

$i$	$Z_i$	$\omega_{i,0}$	$\omega_{i,1}$	$\omega_{i,2}$	$\omega_{i,3}$	$\omega_{i,4}$	$\omega_{i,5}$
1	0.001	2.114	546.6	0	0	0	0
2	0.2	2.661	19.28	-294.3	2292	-8752	13011
3	0.875	3.241	0.238	0	0	0	0
4	0.92	3.241	0.238	0	0	0	0
5	0.95	3.509	6.518	-172	1480	0	0
6	1	3.590	0.204	0	0	0	0

Table C.5: Parameters of the open circuit voltage curve from Equation (C.1).

Figure C.12 shows the piece-wise polynomial representation of the open-circuit curve defined by Equation (C.1) as well as the data points used for the fitting and the moving average fit of those points. It can be seen that this curve is continuous but its gradient is not at all junctions. The function was created to be monotonically increasing, which is generally realistic [57], as it was hypothesised that ensuring monotonicity of this curve would aid in solving the fast charging optimisation problems.

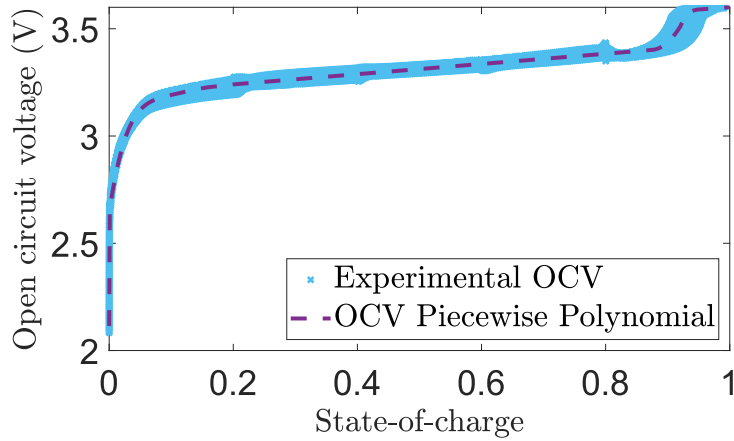


Figure C.12: Comparison between the modelled open circuit voltage curve as a function of state-of-charge from Equation (C.1) with that predicted from the data of [36].

### Appendix D. Cycles to failure predictor

Table D.6 contains the trained values of the vector  $\mathbf{w}$  from Equation (26).

$w_1$	$w_2$	$w_3$	$w_4$	$w_5$	$w_6$	$w_7$	$w_8$	$w_9$
-2625.19	358.30	-1642.00	-985.47	8568.65	-3313.98	2239.72	1516.68	6296.58

Table D.6: Table displaying the values of the trained weights for predicting cycles to failure using Equation (26).

## Appendix E. Method work-flow

Figure E.13 shows the workflow of the proposed method for optimising health-aware fast charging protocols by combining both model-based and data-driven approaches. This work-flow allows the method to be adaptive in the sense that, as new cycling data is generated, the parameters of the model and the degradation cost function can be re-learned using the parameter derivation method above and (26) before the optimisation problem of (16) is re-solved to compute new charging protocols. In this way, the optimised fast charging protocols can evolve in response to the cell ageing.

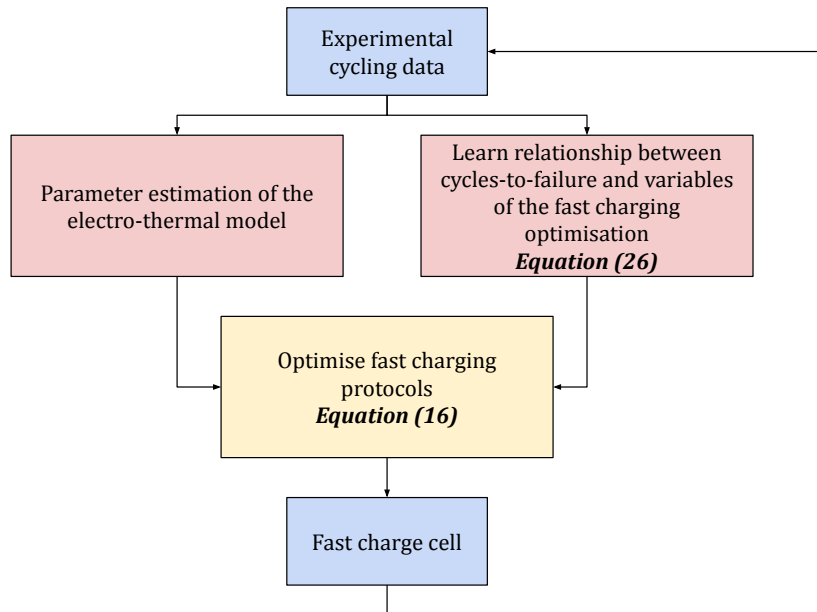


Figure E.13: Illustration of the proposed method to generate optimal fast charging protocols. From experimental data, the method learns a relationship between the cell's cycles-to-failure and the decision variables of the fast charging problem and it also estimates the parameters of an electro-thermal battery model. It then solves a model-based optimal control problem to generate optimised fast charging protocols that minimise the impact on the cell's health.

## References

- [1] J. Turner, E. R. Buiel, Extreme fast charging lithium-ion batteries, Tech. rep., Coulometrics, LLC (2020).
- [2] X.-G. Yang, T. Liu, Y. Gao, S. Ge, Y. Leng, D. Wang, C.-Y. Wang, Asymmetric temperature modulation for extreme fast charging of lithium-ion batteries, *Joule* 3 (12) (2019) 3002–3019.
- [3] A. Tomaszewska, Z. Chu, X. Feng, S. O’Kane, X. Liu, J. Chen, C. Ji, E. Endler, R. Li, L. Liu, et al., Lithium-ion battery fast charging: A review, *ETransportation* 1 (2019) 100011.
- [4] H. Tu, H. Feng, S. Srdic, S. Lukic, Extreme fast charging of electric vehicles: A technology overview, *IEEE Transactions on Transportation Electrification* 5 (4) (2019) 861–878.
- [5] E. J. Dufek, D. P. Abraham, I. Bloom, B.-R. Chen, P. R. Chinnam, A. M. Colclasure, K. L. Gering, M. Keyser, S. Kim, W. Mai, et al., Developing extreme fast charge battery protocols-A review spanning materials to systems, *Journal of Power Sources* (2022) 231129.
- [6] S. Nejad, D. Gladwin, D. Stone, A systematic review of lumped-parameter equivalent circuit models for real-time estimation of lithium-ion battery states, *Journal of Power Sources* 316 (2016) 183–196.
- [7] M. Doyle, T. F. Fuller, J. Newman, Modeling of galvanostatic charge and discharge of the lithium/polymer/insertion cell, *Journal of the Electrochemical society* 140 (6) (1993) 1526–1533.
- [8] A. M. Bizeray, S. Zhao, S. R. Duncan, D. A. Howey, Lithium-ion battery thermal-electrochemical model-based state estimation using orthogonal collocation and a modified extended Kalman filter, *Journal of Power Sources* 296 (2015) 400–412.
- [9] V. Srinivasan, J. Newman, Design and optimization of a natural graphite/iron phosphate lithium-ion cell, *Journal of the Electrochemical Society* 151 (10) (2004) A1530.
- [10] T. S. Chadha, B. Suthar, D. Rife, V. R. Subramanian, P. Biswas, Model based analysis of one-dimensional oriented lithium-ion battery electrodes, *Journal of The Electrochemical Society* 164 (11) (2017) E3114.
- [11] T. Danner, M. Singh, S. Hein, J. Kaiser, H. Hahn, A. Latz, Thick electrodes for Li-ion batteries: A model based analysis, *Journal of Power Sources* 334 (2016) 191–201.
- [12] R. Drummond, C. Cheng, P. Grant, S. Duncan, Modelling the impedance response of graded LiFePO<sub>4</sub> cathodes for Li-Ion batteries, *Journal of The Electrochemical Society* 169 (1) (2022) 010528.
- [13] R. Methekar, V. Ramadesigan, R. D. Braatz, V. R. Subramanian, Optimum charging profile for lithium-ion batteries to maximize energy storage and utilization, *ECS Transactions* 25 (35) (2010) 139.
- [14] R. Klein, N. A. Chaturvedi, J. Christensen, J. Ahmed, R. Findeisen, A. Kojic, Optimal charging strategies in lithium-ion battery, in: *Procs. of the American Control Conference, IEEE, 2011*, pp. 382–387.
- [15] N. E. Courtier, R. Drummond, P. Ascencio, L. D. Couto, D. A. Howey, Discretisation-free battery fast-charging optimisation using the measure-moment approach, in: *European Control Conference (ECC), IEEE, 2022*, pp. 628–634, London, UK.
- [16] H. E. Perez, X. Hu, S. Dey, S. J. Moura, Optimal charging of Li-ion batteries with coupled electro-thermal-aging dynamics, *IEEE Transactions on Vehicular Technology* 66 (9) (2017) 7761–7770.
- [17] B. Jiang, M. D. Berliner, K. Lai, P. A. Asinger, H. Zhao, P. K. Herring, M. Z. Bazant, R. D. Braatz, Fast charging design for lithium-ion batteries via bayesian optimization, *Applied Energy* 307 (2022) 118244.
- [18] S. Park, A. Pozzi, M. Whitmeyer, H. Perez, A. Kandel, G. Kim, Y. Choi, W. T. Joe, D. M. Raimondo, S. Moura, A deep reinforcement learning framework for fast charging of Li-ion batteries, *IEEE Transactions on Transportation Electrification* 8 (2) (2022) 2770–2784.
- [19] C. Chen, Z. Wei, A. C. Knoll, Charging optimization for Li-ion battery in electric vehicles: A review, *IEEE Transactions on Transportation Electrification* (2021).
- [20] C. Zou, C. Manzie, D. Nešić, Model predictive control for lithium-ion battery optimal charging, *IEEE/ASME Transactions on Mechatronics* 23 (2) (2018) 947–957.
- [21] A. Bills, M. Salazar, D. Zhang, V. Viswanathan, A model predictive control scheme for fast charging via accurate quadratic battery models, in: *Procs. of the American Control Conference, IEEE, 2022*, pp. 1794–1800.
- [22] A. Pozzi, S. Moura, D. Toti, A deep learning-based predictive controller for the optimal charging of a lithium-ion cell with non-measurable states, *Computers & Chemical Engineering* 173 (2023) 108222.
- [23] Y. Li, T. Wik, Y. Huang, C. Zou, Nonlinear model inversion-based output tracking control for battery fast charging, *IEEE Transactions on Control Systems Technology* (2023).
- [24] S. Sattarzadeh, S. K. Padisala, Y. Shi, P. P. Mishra, K. Smith, S. Dey, Feedback-based fault-tolerant and health-adaptive optimal charging of batteries, *Applied Energy* 343 (2023) 121187.
- [25] Y. Li, D. M. Vilathgamuwa, E. Wikner, Z. Wei, X. Zhang, T. Thiringer, T. Wik, C. Zou, Electrochemical model-based fast charging: Physical constraint-triggered PI control, *IEEE Transactions on Energy Conversion* 36 (4) (2021) 3208–3220.
- [26] M. D. Berliner, B. Jiang, D. A. Cogswell, M. Z. Bazant, R. D. Braatz, Novel operating modes for the charging of lithium-ion batteries, *Journal of The Electrochemical Society* 169 (10) (2022) 100546.
- [27] P. Mohtat, S. Pannala, V. Sulzer, J. B. Siegel, A. G. Stefanopoulou, An algorithmic safety VEST for Li-ion batteries during fast charging, *IFAC-PapersOnLine* 54 (20) (2021) 522–527.
- [28] K. Zhang, J. Zhou, F. Yang, Y. Zhang, Y. Pan, B. Zheng, Y. Li, F. Yang, A stress-control charging method with multi-stage currents for silicon-based lithium-ion batteries: Theoretical analysis and experimental validation, *Journal of Energy Storage* 56 (2022) 105985.
- [29] Z. M. Konz, P. J. Weddle, P. Gasper, B. D. McCloskey, A. M. Colclasure, Voltage-based strategies for preventing battery degradation under diverse fast-charging conditions, *ACS Energy Letters* 8 (2023) 4069–4077.
- [30] R. Romagnoli, L. D. Couto, A. Goldar, M. Kinnaert, E. Garone, A feedback charge strategy for Li-ion battery cells based on reference governor, *Journal of process control* 83 (2019) 164–176.
- [31] D. Lee, B. Kim, C. B. Shin, Modeling fast charge protocols to prevent lithium plating in a lithium-ion battery, *Journal of The Electrochemical Society* 169 (9) (2022) 090502.
- [32] Y. Cai, C. Zou, Y. Li, T. Wik, Fast charging control of lithium-ion batteries: Effects of input, model, and parameter uncertainties, in: *2022 European Control Conference (ECC), IEEE, 2022*, pp. 1647–1653.

- [33] J. Matschek, M. D. Berliner, A. Himmel, R. D. Braatz, R. Findeisen, Necessary optimality conditions for fast lithium-ion battery charging via hybrid simulations, in: *Procs. of the American Control Conference*, IEEE, 2023, pp. 3783–3789.
- [34] S. Park, D. Lee, H. J. Ahn, C. Tomlin, S. Moura, Optimal control of battery fast charging based-on Pontryagin’s minimum principle, in: *IEEE Conference on Decision and Control (CDC)*, IEEE, 2020, pp. 3506–3513.
- [35] R. Drummond, N. E. Courtier, D. A. Howey, L. D. Couto, C. Guiver, Constrained optimal control of monotone systems with applications to battery fast-charging, *arXiv preprint arXiv:2301.07461* (2023).
- [36] P. M. Attia, A. Grover, N. Jin, K. A. Severson, T. M. Markov, Y.-H. Liao, M. H. Chen, B. Cheong, N. Perkins, Z. Yang, et al., Closed-loop optimization of fast-charging protocols for batteries with machine learning, *Nature* 578 (7795) (2020) 397–402.
- [37] P. Fermín-Cueto, E. McTurk, M. Allerhand, E. Medina-Lopez, M. F. Anjos, J. Sylvester, G. Dos Reis, Identification and machine learning prediction of knee-point and knee-onset in capacity degradation curves of lithium-ion cells, *Energy and AI* 1 (2020) 100006.
- [38] V. Sulzer, P. Mohtat, A. Aitio, S. Lee, Y. T. Yeh, F. Steinbacher, M. U. Khan, J. W. Lee, J. B. Siegel, A. G. Stefanopoulou, et al., The challenge and opportunity of battery lifetime prediction from field data, *Joule* 5 (8) (2021) 1934–1955.
- [39] L. Ward, S. Babinec, E. J. Dufek, D. A. Howey, V. Viswanathan, M. Aykol, D. A. Beck, B. Blaiszik, B.-R. Chen, G. Crabtree, et al., Principles of the battery data genome, *Joule* (2022).
- [40] Q. Lin, J. Wang, R. Xiong, W. Shen, H. He, Towards a smarter battery management system: A critical review on optimal charging methods of lithium ion batteries, *Energy* 183 (2019) 220–234.
- [41] N. Yang, Y. Fu, H. Yue, J. Zheng, X. Zhang, C. Yang, J. Wang, An improved semi-empirical model for thermal analysis of lithium-ion batteries, *Electrochimica Acta* 311 (2019) 8–20.
- [42] T. F. Fuller, M. Doyle, J. Newman, Simulation and optimization of the dual lithium ion insertion cell, *Journal of the electrochemical society* 141 (1) (1994) 1–10.
- [43] W. Allafi, C. Zhang, K. Uddin, D. Worwood, T. Q. Dinh, P. A. Ormeno, K. Li, J. Marco, A lumped thermal model of lithium-ion battery cells considering radiative heat transfer, *Applied Thermal Engineering* 143 (2018) 472–481.
- [44] J. Lin, H. N. Chu, D. A. Howey, C. W. Monroe, Multiscale coupling of surface temperature with solid diffusion in large lithium-ion pouch cells, *Communications Engineering* 1 (1) (2022) 1–10.
- [45] X. Lin, Adaptive estimation of thermal dynamics and charge imbalance in battery strings., Ph.D. thesis (2014).
- [46] A. K. de Souza, G. Plett, M. S. Trimboli, Lithium-ion battery charging control using a coupled electro-thermal model and model predictive control, in: *Applied Power Electronics Conference and Exposition (APEC)*, IEEE, 2020, pp. 3534–3539, Orlando, FL.
- [47] X. Lin, H. E. Perez, S. Mohan, J. B. Siegel, A. G. Stefanopoulou, Y. Ding, M. P. Castanier, A lumped-parameter electro-thermal model for cylindrical batteries, *Journal of Power Sources* 257 (2014) 1–11.
- [48] G. L. Plett, Battery management systems, Volume I: Battery modeling, Artech House, Norwood, MA, 2015.
- [49] A123Systems, APR18650M1A datasheet, <https://www.batteryspace.com/prod-specs/6612.pdf>, online (Last accessed 15 March 2022) (2009).
- [50] M. A. Fischler, R. C. Bolles, Random sample consensus: a paradigm for model fitting with applications to image analysis and automated cartography, *Communications of the ACM* 24 (6) (1981) 381–395.
- [51] MathWorks, Matlab help center: greyest, <https://www.mathworks.com/help/ident/ref/iddata.greyest.html>, online (Last accessed 24 March 2022) (2022).
- [52] C. R. Birkel, M. R. Roberts, E. McTurk, P. G. Bruce, D. A. Howey, Degradation diagnostics for lithium ion cells, *Journal of Power Sources* 341 (2017) 373–386.
- [53] P. M. Attia, A. Bills, F. B. Planella, P. Dechent, G. Dos Reis, M. Dubarry, P. Gasper, R. Gilchrist, S. Greenbank, D. Howey, et al., “knees” in lithium-ion battery aging trajectories, *Journal of The Electrochemical Society* 169 (6) (2022) 060517.
- [54] L. Liu, M. Zhu, Modeling of SEI layer growth and electrochemical impedance spectroscopy response using a thermal-electrochemical model of Li-ion batteries, *ECS Transactions* 61 (27) (2014) 43.
- [55] M. A. Cabanero, J. Altmann, L. Gold, N. Boaretto, J. Müller, S. Hein, J. Zausch, J. Kallo, A. Latz, Investigation of the temperature dependence of lithium plating onset conditions in commercial Li-ion batteries, *Energy* 171 (2019) 1217–1228.
- [56] MathWorks, Matlab help center: fmincon, <https://www.mathworks.com/help/optim/ug/fmincon.html>, online (Last accessed 15 February 2022) (2022).
- [57] R. Zhang, B. Xia, B. Li, L. Cao, Y. Lai, W. Zheng, H. Wang, W. Wang, M. Wang, A study on the open circuit voltage and state of charge characterization of high capacity lithium-ion battery under different temperature, *Energies* 11 (9) (2018) 2408.